



**HAL**  
open science

## Mapping electric fields in real nanodevices by operando electron holography

Maria Brodovoi, Kilian Gruel, Aurélien Masseboeuf, Lucas Chapuis, Martin Hÿtch, Frédéric Lorut, Christophe Gatel

► **To cite this version:**

Maria Brodovoi, Kilian Gruel, Aurélien Masseboeuf, Lucas Chapuis, Martin Hÿtch, et al.. Mapping electric fields in real nanodevices by operando electron holography. *Applied Physics Letters*, 2022, 120 (23), pp.233501. 10.1063/5.0092019 . hal-03752638

**HAL Id: hal-03752638**

**<https://hal.science/hal-03752638>**

Submitted on 17 Aug 2022

**HAL** is a multi-disciplinary open access archive for the deposit and dissemination of scientific research documents, whether they are published or not. The documents may come from teaching and research institutions in France or abroad, or from public or private research centers.

L'archive ouverte pluridisciplinaire **HAL**, est destinée au dépôt et à la diffusion de documents scientifiques de niveau recherche, publiés ou non, émanant des établissements d'enseignement et de recherche français ou étrangers, des laboratoires publics ou privés.

# Mapping electric fields in real nanodevices by *operando* electron holography

Maria Brodovoi<sup>1,2</sup>, Kilian Gruel<sup>1</sup>, Aurélien Masseboeuf<sup>1</sup>, Lucas Chapuis<sup>1</sup>, Martin Hÿtch<sup>1</sup>, Frédéric Lorut<sup>2</sup>, Christophe Gatel<sup>1,3,\*</sup>

<sup>1</sup> CEMES-CNRS, 29 rue Jeanne Marvig, 31055, Toulouse, France

<sup>2</sup> STMicroelectronics, 850 rue Jean Monnet, 38920 Crolles, France

<sup>3</sup> University Toulouse III – Paul Sabatier, 118 route de Narbonne, 31062 Toulouse, France

\*Corresponding author: christophe.gatel@cemes.fr

Keywords: Transmission electron microscopy, electron holography, focused ion beam sample preparation, Circuit edition, nano-electronic, devices, nanocapacitors, electrical properties, finite element modelling

## 1 Abstract

2 Nano-electronic devices play an essential role in many  
3 domains, and their development and improvement attract  
4 considerable attention in fundamental and applied research.  
5 Access to the local physical processes involved in these  
6 nanosystems during their operation is therefore crucial. We  
7 show how electric fields in real nanodevices can be studied  
8 under working conditions using *operando* electron  
9 holography. A specific sample preparation method was first  
10 developed to bias electron-transparent nanodevices  
11 extracted from production lines whilst ensuring their  
12 electrical connectivity and functionality without employing  
13 dedicated probe-based holders. Metal-insulator-metal  
14 (MIM) nanocapacitors were prepared using this approach  
15 based on focused ion beam (FIB) circuit modification.  
16 *Operando* electron holography allowed the electric potential  
17 to be quantitatively mapped in the active areas, and between  
18 devices, whilst biasing the devices *in situ*. Experimental  
19 results were compared with finite element method (FEM)  
20 modelling simulations to determine local electrical  
21 parameters. We demonstrate that electrical properties such  
22 as capacitance and surface charge density can be measured  
23 at the nanoscale and have been preserved by our sample  
24 preparation methodology when compared to macroscopic  
25 measurements. This work paves the way for mapping the  
26 local electrical properties of more complex biased devices.  
27

## 28 Main text

29 The development of nanometer-scaled electronic  
30 devices with reduced dimensions, involving new materials  
31 or new architectures such as Magnetic Random Access  
32 Memories (MRAM)<sup>1-4</sup>, memristors<sup>5-7</sup> or Phase Change  
33 Memories (PCM)<sup>8-12</sup>, requires a deeper understanding of  
34 their operating properties. While electrical and physical  
35 characterizations are widely used to monitor and evaluate  
36 both the device performance and the quality of the layer  
37 stack, there is a lack of knowledge on how the  
38 electromagnetic fields are precisely mediated along devices  
39 at the nanoscale level. Correlating local electric fields

40 mapped across a chosen device with its structural properties  
41 and chemical composition would greatly help research  
42 laboratories and the microelectronics industry in the  
43 development of new nano-electronic devices. Furthermore,  
44 these local studies could also provide methods to determine  
45 the root causes of electrical failure<sup>13</sup> to improve the devices  
46 in terms of reliability, speed and power consumption.

47 Transmission Electron Microscopy (TEM) is a powerful  
48 technique for studying the properties of individual  
49 nanosystems with very high spatial resolution. Among TEM  
50 methods, off-axis Electron Holography (EH) is an  
51 interferometric technique that allows quantitative mapping  
52 of electrical potentials inside and around the specimen, as  
53 well as the measurement of charge distributions<sup>14-18</sup> with a  
54 precision down to the elementary charge.<sup>19</sup> EH  
55 experiments, when combined with *in situ* biasing, pave the  
56 way for nanoscale studies of fundamental electrical  
57 phenomena of nanodevices in working conditions.  
58 However, despite these exciting prospects, *operando* EH has  
59 been used relatively little to investigate the local properties  
60 of nanosystems. A few model systems (nano tips<sup>20-24</sup>,  
61 quantum wells<sup>25</sup>, nanowires<sup>26,27</sup>, p-n junctions<sup>28-31</sup>, oxide  
62 layers<sup>32</sup>) have been studied, but key issues such as specimen  
63 preparation, surface damage layers, stray field and electron  
64 radiation were identified.<sup>30,33,34</sup> The investigation of real  
65 devices are rarer still<sup>35,36</sup>, even with dedicated probe-based  
66 holders.<sup>37</sup> The main problem is that stray fields around the  
67 nanoprobe may interfere with the reference wave required  
68 in holography<sup>21</sup> and the potential applied to the active area.<sup>38</sup>  
69 In addition, the contact resistance between nanoprobe and  
70 sample is unknown, poorly controllable and causes  
71 mechanical instabilities.

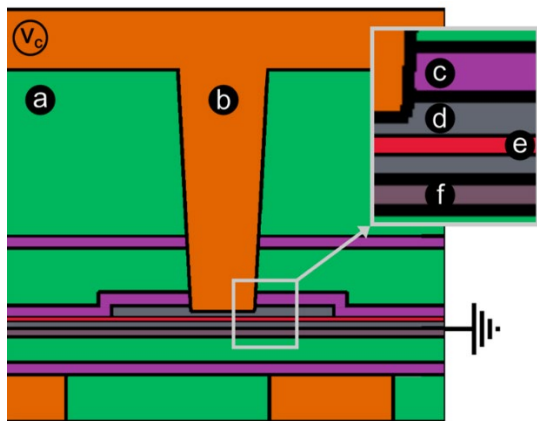
72 *In situ* biasing TEM experiments thus necessitate a  
73 specific and complex sample preparation that minimizes  
74 preparation artifacts whilst ensuring the electrical  
75 functionality of the nanodevice itself. A dedicated setup for  
76 applying bias from the macroscopic to nanometre scale is  
77 also required to avoid electrostatic discharge that can  
78 destroy the fragile specimen. Moreover, the signal from  
79 local charge distributions is extremely weak and measuring  
80 such a signal on a working device prepared by sample

81 preparation methods such focused-ion beam (FIB) is very  
82 challenging. Finally, the analysis of the resulting phase  
83 images remains complex due to the integration of the signal  
84 along the electron path as well as additional effects (beam-  
85 induced charge, stray fields and sample preparation  
86 artifacts).

87 Here we present the methodology that we have been  
88 developing for mapping the electrical properties of nano-  
89 electronic devices extracted directly from production lines  
90 without using a probe-based approach. We investigated the  
91 potential distribution at the nanoscale of metal-insulator-  
92 metal (MIM) nanocapacitors using advanced FIB sample  
93 preparation and state-of-the-art EH. Capacitors are, in fact,  
94 one of the most important components in all electronic  
95 devices. They are widely used in analog and RF circuit  
96 applications for energy storage and delivery in memory  
97 devices such as flash memories and random access memory  
98 (RAM) chips, and processors whose performance is  
99 dependent on their miniaturization and operation.  
100 Experimental phase measurements will be compared to  
101 additional numerical simulations using finite element  
102 modelling (FEM) including factors such as specimen  
103 geometry and stray fields.

104 Our results demonstrate that electrical properties such  
105 as electric field, capacitance and surface charge density can  
106 be preserved and investigated at the nanoscale.

107 Experiments were carried out on an array of parallel  
108 MIM nanocapacitors extracted from a matrix structure  
109 integrated in a STMicroelectronics 28 nm process test chip.  
110 The nanocapacitors used in backend upper layers for high  
111 frequency circuit applications are made up of a thin 11.5 nm  
112 tantalum pentoxide ( $\text{Ta}_2\text{O}_5$ ) high- $k$  insulator sandwiched  
113 between two TiN electrodes connected to a Cu pillar  
114 (above) and a Al layer (below) (Fig. 1). The upper electrode  
115 of TiN has a width of 950 nm (in the plane of the image)  
116 and 1.7  $\mu\text{m}$  in depth (out-of-plane).



119  
120  
121  
122  
123  
124  
125  
126  
127  
128  
129  
130  
131  
132  
133  
134  
135  
136  
137  
138  
139  
140  
141  
142  
143  
144  
145  
146  
147  
148  
149  
150  
151  
152  
153  
154  
155  
156  
157  
158  
159  
160  
161  
162

FIG. 1. Architecture of MIM nanocapacitor: (a)  $\text{SiO}_2$ , (b) Cu interconnects; (c)  $\text{Si}_3\text{N}_4$ ; (d) TiN electrodes; (e) active region of  $\text{Ta}_2\text{O}_5$  dielectric; (f) Al electrode.

Prior to experiments, individual MIM of the array were measured to have a capacitance of  $35 \pm 2 \text{ fF}$  at 1 MHz using a nanoprobe (nProber III from ThermoFisher). Assuming the formula for a parallel plate capacitor with a surface area corresponding to the top TiN electrode gives a relative electric permittivity of the thin-layer  $\text{Ta}_2\text{O}_5$  to be  $28 \pm 1$ , which is in the range of values found in the literature.<sup>40</sup>

The specimen-device for holography experiments was prepared using a dual-beam FIB (Helios NanoLab 1200AT DualBeam from ThermoFisher) with a gallium liquid-metal ion source and gas injection system (GIS). A slab of material containing the MIM array was lifted from a fully processed wafer and prepared for electron transparency and *in situ* biasing (Fig. 2).

To ensure proper charge evacuation during specimen navigation and preparation, a thin conductive layer of gold-palladium alloy was deposited on the sample surface prior to extraction. The specimen surface was then connected to the Si substrate by milling a hole in the pad, allowing the charge from the electron beam to drain to the ground. Top and bottom electrodes were also temporarily connected by Pt deposition to prevent electrostatic discharges harming the nanocapacitors during the deprocessing. The specimen-device was then deprocessed top-down with FIB until the copper lines connecting the nanocapacitors were exposed.

A second layer of Pt was deposited to equalize the potential of the two electrodes reconstructing the top circuit, and to protect the structure during further milling. The lamella was then cut and extracted from the wafer and placed on a dedicated chip (Hummingbird Scientific) over a trench surrounded by the prepatterned Au tracks (Fig. 2(a)) before being welded by W deposition using GIS at both ends to ensure the electrical connection (Fig. 2(b)).

Final thinning of the lamella was performed with a low energy ion beam (8 kV) to minimize the impact of surface damage on the thin device compared to the corresponding embedded device. A uniform thickness of about 100 nm was then obtained for two of the capacitors in the array (Figures 2(c) and 2(d)). The final step in the preparation process was to cut trenches so that the top and the bottom electrodes could be biased independently.

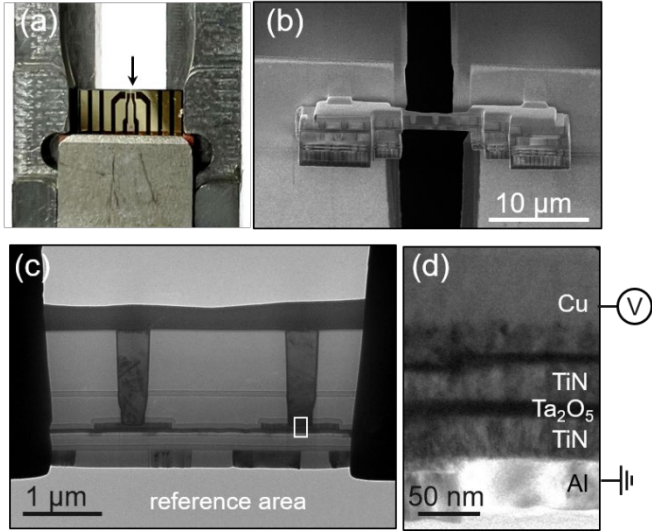


FIG. 2. MIM nanocapacitor specimen-device prepared for operando EH study: (a) chip inserted in sample holder (arrow indicates position of MIM nanocapacitors); (b) SEM image of sample device connected to gold electrodes on chip; (c) TEM image of final specimen-device active area; (d) enlargement of MIM nanocapacitor showing stack.

Such specimen-devices are extremely delicate, with capacitances estimated to be only around 2 fF (the cross-sectional area of the dielectric in the thin lamella is 17 times smaller of the original device). An additional setup consisting of several levels of electrical connections with adapted equipment and software, was therefore developed to protect the thinned nanocapacitors from electrical discharge. Indeed, the electrical resistance of completed specimen-devices was measured prior to TEM experiments to confirm that the nanocapacitors had not been electrically shorted. The chip supporting the connected devices was inserted into a Hummingbird holder designed specifically for biasing experiments (1600 series, Hummingbird scientific) and connected to this additional setup. The bottom electrode was grounded whilst positive, negative or zero biases were applied *in situ* to the top electrode for the electron holography experiments.

The principle of off-axis electron holography is to use an electrostatically charged wire to interfere a beam of highly coherent electrons that has interacted with the specimen, called “object wave”, with a reference wave that has not undergone interaction with any field.<sup>41–43</sup> The resulting interference pattern (*i.e.* the hologram) contains all of information on the phase shift of the electron wave experienced when interacting with the local electromagnetic fields.<sup>14,43</sup>

The electrical potential  $V$  distribution induces a phase shift  $\phi$  recorded in the  $x$ - $y$  image plane:<sup>44–46</sup>

$$\phi(x, y) = C_E \int V(x, y, z) dz \quad (1)$$

where  $C_E$  is an energy-related constant that depends on the accelerating voltage ( $6.526 \cdot 10^6 \text{ V}^{-1} \cdot \text{m}^{-1}$  at 300kV) and  $\xi$  the direction of the electron path.  $V$  is the sum of the mean internal potential  $V_{MIP}$ , which is related to the atomic potential and static charges, and  $V_{Bias}$ , which is caused by the applied bias. As a result,  $\phi$  can be divided into two sub-contributions,  $\phi_{MIP}$ , and  $\phi_{Bias}$ . Since  $\phi_{MIP}$  does not depend on the bias, it can be measured by grounding the two electrodes and subtracted from the total measured phase shift. It is then possible to isolate  $\phi_{Bias}$  on applying bias.

*Operando* EH experiments were carried out on a Hitachi HF3300-C (I2TEM) microscope specifically designed for *in situ* electron interferometry studies. It is equipped with a cold field-emission gun (CFEG) for optimal brightness and an imaging aberration corrector (BCOR from CEOS), which allows on- and off-axis aberrations to be corrected over wide fields of view. Observations were performed with the microscope operating at 300 kV in Lorentz mode with a spatial resolution of 0.5 nm<sup>47</sup>, elliptical illumination and 2 post-specimen biprisms to avoid artefacts linked to Fresnel fringes and to allow adjustment of the interference area with respect to the fringe spacing.<sup>48</sup> The reference wave was placed in the field-free region of the vacuum beneath the Al electrode (cf Fig. 2(c)).

A high-speed 4k by 4k camera (OneView, Gatan Inc.) operating at full-frame rate of 25 images per second was used with a temporal integration window of 250 ms, which corresponds to the sum of the frames displayed in the previous 250 ms. Holograms with an interfringe of 1.5 nm (5 pixels) were acquired using dynamic automation<sup>49</sup> and  $\pi$ -shift method<sup>50</sup> over a total exposure time of 120 s each corresponding to the sum of 480 images.

The phase was monitored in real-time during experiments using HoloLive 1.0 (HREM Research Inc.), a plug-in for the image processing package Digital Micrograph (GMS 3.3, Gatan Inc.). In-house scripts and dedicated code implemented within Digital Micrograph were used to analyze the holograms and extract amplitude and phase images during post-processing. A 5<sup>th</sup> order Butterworth Fourier-space filter centered on the sideband giving a spatial resolution of 3 nm was selected for the amplitude and phase images. To remove the projector and camera distortion-induced phase modulations, a dedicated reference hologram recorded in a vacuum area was used. For each applied bias, a final field of view of  $3.5 \mu\text{m} \times 1 \mu\text{m}$  was reconstructed by aligning and combining 3 images.

Figures 3(a) and 3(b) show the experimental amplitude and phase images, respectively, acquired with 0.6 V of bias applied by the power supply. The phase image only contains the electrostatic contribution  $\phi_{Bias}$  from biasing. The mean phase and linear phase ramp measured within the bottom



245 substrate were subtracted from the whole phase image. 275  
 246 Isophase contours with a spacing of 0.25 rad, calculated 276  
 247 from the phase image, have been superimposed on the  
 248 amplitude image.

249 On biasing, the phase presents a sharp variation across  
 250 the Ta<sub>2</sub>O<sub>5</sub> layer due to the strong local electrical field in the  
 251 dielectric, but is relatively uniform within the electrodes, as  
 252 expected. There is also an in-plane stray field between the  
 253 nanocapacitors due to the finite lateral dimensions of the  
 254 upper electrodes (zoom in Fig. 3(b)). This weak stray field  
 255 is clearly visible because of the very long exposure times of  
 256 our automated holography experiments.<sup>49</sup>  
 257

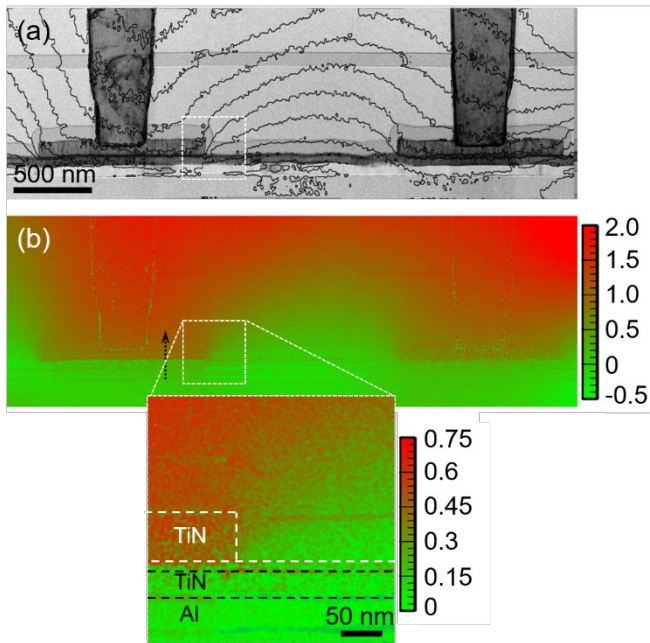


FIG. 3. Operando electron holography: (a) Amplitude image of both MIM nanocapacitors in parallel; (b) Experimental phase image of the induced electrostatic potential for 0.6 V bias applied by the power supply.

258  
 259 To analyze quantitatively the potential distribution  
 260 across the thin oxide layer, profiles were plotted from the  
 261 phase images along the black arrow (Fig. 3(b)) for different  
 262 biases and averaged over a width of 50 nm parallel to the  
 263 interfaces (Fig. 4). The overall phase shift across the  
 264 dielectric increases linearly with applied bias, as expected  
 265 from Equation (1). On the other hand, the phase is not  
 266 completely flat in the electrodes whereas we would expect  
 267 them to be at a uniform potential.

268 In fact, the phase curvature is caused by the stray field  
 269 above and below the thin lamella since the phase is  
 270 integrated along the whole path of the electron beam (cf Eq.  
 271 (1)), inside and outside the specimen. Unfortunately, the  
 272 stray field cannot be described analytically for complex  
 273 geometries so numerical modeling must be performed to  
 274 separate the effects of the internal and external fields.

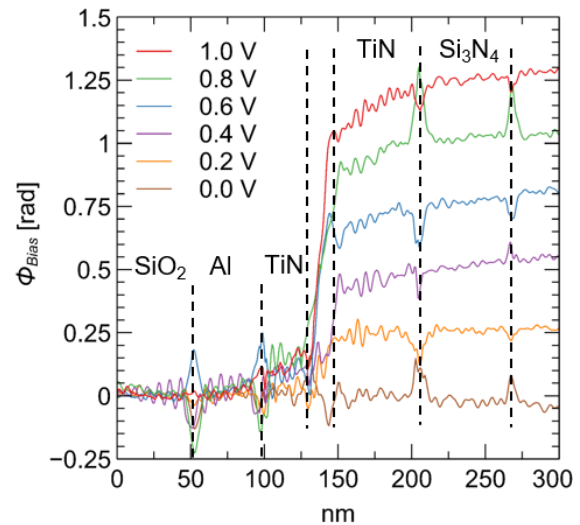


FIG. 4. Phase profiles extracted along the black dotted arrow in Fig. 3(b) for different biases. Ta<sub>2</sub>O<sub>5</sub> active layer is between the two TiN electrodes.

277

278

279

280 Three-dimensional (3D) finite element method (FEM)  
 281 modeling was performed with the COMSOL software  
 282 package (COMSOL Multiphysics). The model geometry  
 283 and dimensions were based on the TEM images of the  
 284 observed devices, to approach the reality of the experiments  
 285 as closely as possible. Indeed, this is one of the advantages  
 286 of TEM experiments that accurate digital twins can be built  
 287 relatively easily. The main uncertainty is the exact lamella  
 288 thickness, which we measured by electron energy-loss  
 289 spectroscopy (EELS) to be 100 ± 10 nm based on theoretical  
 290 mean-free paths for elastic scattering.

291

292

293

294

295

296

297

298

299

300

301

302

303

304

305

306

307

To convert this into a potential, the phase change across the

308 dielectric was determined from the simulated curves. The  
 309 result of  $0.88 \text{ rad.V}^{-1}$  means that the phase error is  
 310 equivalent to about 60 mV of applied bias. Simulations also  
 311 confirm that the out-of-plane stray field is indeed the cause  
 312 of the non-uniform phase in the region corresponding to  
 313 the electrodes. Even the in-plane stray field is well  
 314 reproduced (see Fig. 5(d)) and the simulations of the out-  
 315 of-plane stray field confirm that it is indeed the cause of the  
 316 non-uniform phase in the region corresponding to the  
 317 electrodes.

318 However, in order to obtain this agreement, the local  
 319 applied bias in the model was 0.40V. Indeed, the dominant  
 320 source of uncertainty being the lamella thickness, we can  
 321 estimate the local experimental bias to be within 40 mV of  
 322 this value. The local bias was therefore significantly lower  
 323 than the 0.6V indicated by the external power supply. The  
 324 discrepancy between the bias applied locally and  
 325 macroscopically is most probably caused by leakage currents  
 326 and impedances in the connections.

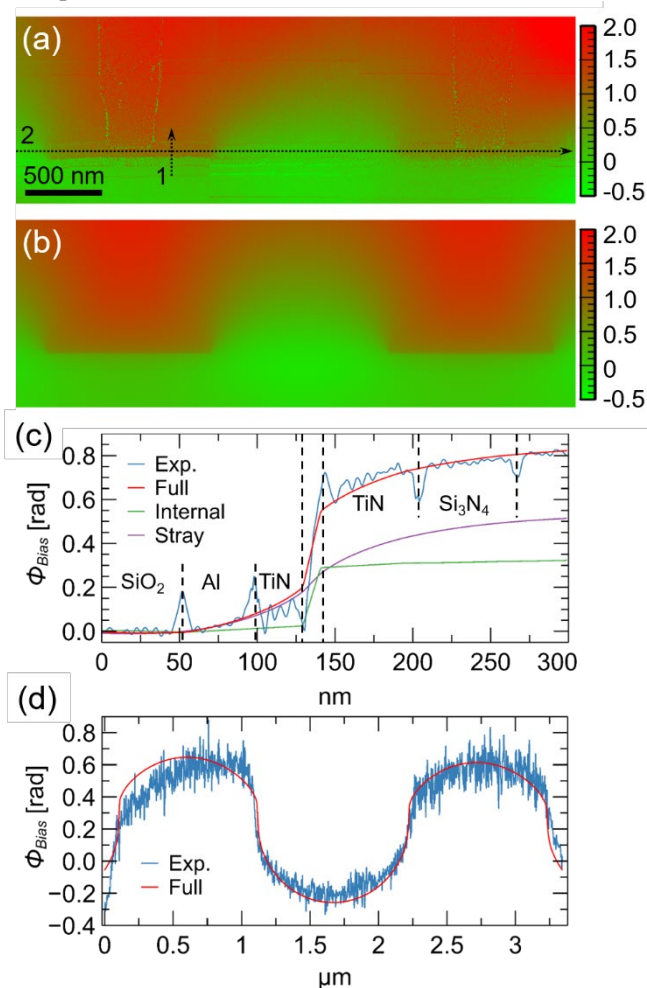


FIG. 5. Quantitative analysis: (a) experimental phase; (b) FEM simulated phase; (c) experimental phase profiles across active layer (black arrow 1), corresponding simulated profiles for the internal field (green), stray field (purple) and

total contribution (red); (d) horizontal phase profiles (black arrow 2).

327

328

329

330

331

332

333

334

335

336

337

338

339

340

341

342

343

344

345

346

347

348

349

350

351

352

353

354

355

356

357

358

359

360

361

362

363

364

365

366

367

368

369

370

371

372

373

374

375

376

The agreement between simulations and experiment means that we can be confident in the local electrical parameters extracted from the model, such as the electrostatic potential inside the dielectric layer, the capacitance, and surface charge density. The electric field inside the dielectric layer was found to be  $0.35 \pm 0.04 \text{ MV cm}^{-1}$  for the specimen-device with a corresponding capacitance of 2.1 fF, very close to the estimated value from macroscopic measurement, even for the DC bias of the EH experiments. The surface charge density is then 0.12 elementary charge per nm<sup>2</sup> and per Volt. The energy associated with the induced electrical field between both electrode plates is equal to  $3.9 \cdot 10^{-16} \text{ J.V}^{-1}$ , while the energy of the stray fields between two neighboring devices corresponds to  $1.24 \cdot 10^{-18} \text{ J.V}^{-1}$ , or 0.3% of the total energy.

These results show that devices extracted from production lines can be prepared for TEM studies whilst preserving their electrical connectivity and functionality. *Operando* electron holography can then be used to quantitatively map the electric potential distribution as a function of bias. That the measured electric field can be modeled with almost no fitting parameters suggests that the device is indeed functioning normally within the microscope.

There is no reason that the same methodology cannot be applied to more complex electronic devices such as MOS transistors or spintronic devices by adapting the sample preparation workflow to achieve a successful circuit modification and enable electrical stimulation of the device. Furthermore, measurements can be correlated to complementary TEM techniques for a full understanding of structural, chemical and electrical properties of individual devices at the nanometer scale. We hope that the ability to study local electric fields quantitatively in newly proposed devices and devices already in production will help efforts to explore fundamental physical processes as well as to develop and improve current devices.

## Acknowledgments

We thank Cécile Marcelot, responsible for the microscopy service at CEMES, for help with the EELS analysis. The authors acknowledge the French National Research Agency under the "Investissement d'Avenir" program reference No. ANR-10-EQPX-38-01" and No. 11-IDEX-0002, the "Conseil Régional Midi-Pyrénées" and the European FEDER for financial support within the CPER program. This work was also supported by the French national

377 project IODA (ANR-17-CE24-0047). This project  
378 (ADVENT - 16ENG06) has received funding from the  
379 EMPIR program co-financed by the Participating States and  
380 from the European Union's Horizon 2020 research and  
381 innovation program. The research leading to these results  
382 has received funding from the European Union Horizon  
383 2020 research and innovation program under grant  
384 agreement No. 823717 – ESTEEM3.

385  
386

## 387 References

388 <sup>1</sup> J.S. Moodera, L.R. Kinder, T.M. Wong, and R. Meservey,  
389 *Phys Rev Lett* **74**, 3273 (1995).  
390 <sup>2</sup> J.C. Slonczewski, *J. Magn. Magn. Mater.* **159**, L1 (1996).  
391 <sup>3</sup> J. Åkerman, *Science* **308**, 508 (2005).  
392 <sup>4</sup> R. Sbiaa, H. Meng, and S.N. Piramanayagam, *Phys. Status*  
393 *Solidi RRL – Rapid Res. Lett.* **5**, 413 (2011).  
394 <sup>5</sup> L. Chua, *IEEE Trans. Circuit Theory* 507 (1971).  
395 <sup>6</sup> D.B. Strukov, G.S. Snider, D.R. Stewart, and R.S. Williams,  
396 *Nature* **453**, 80 (2008).  
397 <sup>7</sup> M.D. Ventra and Y.V. Pershin, *Nanotechnology* **24**, 255201  
398 (2013).  
399 <sup>8</sup> S. Raoux, G.W. Burr, M.J. Breitwisch, C.T. Rettner, Y.C.  
400 Chen, R.M. Shelby, M. Salinga, D. Krebs, S.H. Chen, H.L.  
401 Lung, and C.H. Lam, *IBM J. Res. Dev.* **52**, 465 (2008).  
402 <sup>9</sup> S. Raoux, C.T. Rettner, Y.-C. Chen, and G.W. Burr, *MRS*  
403 *Bull.* **33**, 847 (2008).  
404 <sup>10</sup> D. Krebs, S. Raoux, C.T. Rettner, G.W. Burr, M. Salinga, and  
405 M. Wuttig, *Appl. Phys. Lett.* **95**, 082101 (2009).  
406 <sup>11</sup> G.W. Burr, M.J. Breitwisch, M. Franceschini, D. Garetto, K.  
407 Gopalakrishnan, B. Jackson, B. Kurdi, C. Lam, L.A. Lastras, A.  
408 Padilla, B. Rajendran, S. Raoux, and R.S. Shenoy, *J. Vac. Sci.*  
409 *Technol. B* **28**, 223 (2010).  
410 <sup>12</sup> Y. Jung, S.-W. Nam, and R. Agarwal, *Nano Lett.* **11**, 1364  
411 (2011).  
412 <sup>13</sup> H.J. Engelmann, H. Saage, and E. Zschech, *Microelectron.*  
413 *Reliab.* **40**, 1747 (2000).  
414 <sup>14</sup> P.A. Midgley and R.E. Dunin-Borkowski, *Nat. Mater.* **8**, 271  
415 (2009).  
416 <sup>15</sup> M.R. McCartney, N. Agarwal, S. Chung, D.A. Cullen, M.-G.  
417 Han, K. He, L. Li, H. Wang, L. Zhou, and D.J. Smith,  
418 *Ultramicroscopy* **110**, 375 (2010).  
419 <sup>16</sup> M. McCartney, R.E. Dunin-Borkowski, and D. Smith,  
420 *Ultramicroscopy* **203**, 105 (2019).  
421 <sup>17</sup> M. Beleggia, T. Kasama, R.E. Dunin-Borkowski, S.  
422 Hofmann, and G. Pozzi, *Appl. Phys. Lett.* **98**, 243101 (2011).  
423 <sup>18</sup> M. Beleggia, T. Kasama, D.J. Larson, T.F. Kelly, R.E. Dunin-  
424 Borkowski, and G. Pozzi, *J. Appl. Phys.* **116**, 024305 (2014).  
425 <sup>19</sup> C. Gatel, A. Lubk, G. Pozzi, E. Snoeck, and M. Hÿtch, *Phys.*  
426 *Rev. Lett.* **111**, (2013).  
427 <sup>20</sup> Cumings J., Zettl A., McCartney M.R., and Spence J.C.H.,  
428 *Phys Rev Lett* **88**, 056804 (2002).  
429 <sup>21</sup> L. de Knoop, F. Houdellier, C. Gatel, A. Masseboeuf, M.  
430 Monthieux, and M. Hÿtch, *Micron* **63**, 2 (2014).

431 <sup>22</sup> L. de Knoop, C. Gatel, F. Houdellier, M. Monthieux, A.  
432 Masseboeuf, E. Snoeck, and M.J. Hÿtch, *Appl. Phys. Lett.* **106**,  
433 263101 (2015).  
434 <sup>23</sup> V. Migunov, C. Dwyer, C.B. Boothroyd, G. Pozzi, and R.E.  
435 Dunin-Borkowski, *Ultramicroscopy* **178**, 48 (2017).  
436 <sup>24</sup> K. He and J. Cumings, *Nano Lett.* **13**, 4815 (2013).  
437 <sup>25</sup> L.Z.-Y. Liu, C. McAleese, D.V. Sridhara Rao, M.J. Kappers,  
438 and C.J. Humphreys, *Phys. Status Solidi C* **9**, 704 (2012).  
439 <sup>26</sup> M.I. den Hertog, H. Schmid, D. Cooper, J.-L. Rouviere, M.T.  
440 Björk, H. Riel, P. Rivallin, S. Karg, and W. Riess, *Nano Lett.*  
441 **9**, 3837 (2009).  
442 <sup>27</sup> M. den Hertog, R. Songmuang, and E. Monroy, *J. Phys. Conf.*  
443 *Ser.* **471**, 012019 (2013).  
444 <sup>28</sup> K. He, J.-H. Cho, Y. Jung, S.T. Picraux, and J. Cumings,  
445 *Nanotechnology* **24**, 115703 (2013).  
446 <sup>29</sup> A.C. Twitchett, R.E. Dunin-Borkowski, and P.A. Midgley,  
447 *Phys. Rev. Lett.* **88**, 238302 (2002).  
448 <sup>30</sup> S. Yazdi, T. Kasama, M. Beleggia, M. Samaie Yekta, D.W.  
449 McComb, A.C. Twitchett-Harrison, and R.E. Dunin-  
450 Borkowski, *Ultramicroscopy* **152**, 10 (2015).  
451 <sup>31</sup> A.C. Twitchett-Harrison, R.E. Dunin-Borkowski, and P.A.  
452 Midgley, *Scanning* **30**, 299 (2008).  
453 <sup>32</sup> Y. Yao, C. Li, Z.L. Huo, M. Liu, C.X. Zhu, C.Z. Gu, X.F.  
454 Duan, Y.G. Wang, L. Gu, and R.C. Yu, *Nat. Commun.* **4**,  
455 (2013).  
456 <sup>33</sup> D. Wolf, A. Lubk, A. Lenk, S. Sturm, and H. Lichte, *Appl.*  
457 *Phys. Lett.* **103**, 264104 (2013).  
458 <sup>34</sup> J.B. Park, T. Niermann, D. Berger, A. Knauer, I. Koslow, M.  
459 Weyers, M. Kneissl, and M. Lehmann, *Appl. Phys. Lett.* **105**,  
460 094102 (2014).  
461 <sup>35</sup> T. Goto, J.S. Jeong, W. Xia, Z. Akase, D. Shindo, and K.  
462 Hirata, *Microscopy* **62**, 383 (2013).  
463 <sup>36</sup> J.F. Einsle, C. Gatel, A. Masseboeuf, R. Cours, M.A. Bashir,  
464 M. Gubbins, R.M. Bowman, and E. Snoeck, *Nano Res.* **8**, 1241  
465 (2015).  
466 <sup>37</sup> N. Ikarashi, H. Takeda, K. Yako, and M. Hane, *Appl. Phys.*  
467 *Lett.* **100**, 143508 (2012).  
468 <sup>38</sup> M. Duchamp, V. Migunov, A.H. Tavabi, A. Mehonic, M.  
469 Buckwell, M. Munde, A.J. Kenyon, and R.E. Dunin-  
470 Borkowski, *Resolut. Discov.* **1**, 27 (2016).  
471 <sup>39</sup> N. Ikarashi, H. Takeda, K. Yako, and M. Hane, *Appl. Phys.*  
472 *Lett.* **100**, 143508 (2012).  
473 <sup>40</sup> C. Chaneliere, J.L. Autran, R.A.B. Devine, and B. Balland,  
474 *Mater. Sci. Eng. R Rep.* **22**, 269 (1998).  
475 <sup>41</sup> D. Gabor, *Nature* **161**, 777 (1948).  
476 <sup>42</sup> A. Tonomura, in *Prog. Opt.*, edited by E. Wolf (Elsevier,  
477 1986), pp. 183–220.  
478 <sup>43</sup> A. Tonomura, *Rev. Mod. Phys.* **59**, 639 (1987).  
479 <sup>44</sup> W. Ehrenberg and R.E. Siday, *Proc. Phys. Soc. Sect. B* **62**, 8  
480 (1949).  
481 <sup>45</sup> Y. Aharonov and D. Bohm, *Phys. Rev.* **115**, 485 (1959).  
482 <sup>46</sup> Y. Aharonov and D. Bohm, *Phys. Rev.* **123**, 1511 (1961).  
483 <sup>47</sup> E. Snoeck, F. Houdellier, Y. Taniguch, A. Masseboeuf, C.  
484 Gatel, J. Nicolai, and M. Hÿtch, *Microsc. Microanal.* **20**, 932  
485 (2014).  
486 <sup>48</sup> K. Harada, J. Endo, N. Osakabe, and A. Tonomura, *E-J. Surf.*  
487 *Sci. Nanotechnol.* **6**, 29 (2008).

M. Brodovoi, K. Gruel, A. Masseboeuf, L. Chapuis, M. Hÿtch, F. Lorut, and C. Gatel, **Appl. Phys. Lett.** 120, 233501 (2022). *Mapping electric fields in real nanodevices by operando electron holography*. [10.1063/5.0092019](https://doi.org/10.1063/5.0092019)

488 <sup>49</sup> C. Gatel, J. Dupuy, F. Houdellier, and M.J. Hÿtch, Appl.

489 Phys. Lett. **113**, 133102 (2018).

490 <sup>50</sup> V.V. Volkov, M.G. Han, and Y. Zhu, Ultramicroscopy **134**,

491 175 (2013).

492

493

494